Quaternary Science Reviews 47 (2012) 116–130

Contents lists available at SciVerse ScienceDirect

Quaternary Science Reviews

journal homepage: www.elsevier.com/locate/quascirev

Cosmogenic nuclide age constraints on Middle Stone Age lithics from Niassa, Mozambique

Julio Mercader [a,*], John C. Gosse [b], Tim Bennett [a], Alan J. Hidy [b], Dylan H. Rood [c,d]

[a] Department of Archaeology, University of Calgary, 2500 Univ Dr. NW, Calgary, Alberta T2N 1N4, Canada
[b] Department of Earth Sciences, Dalhousie University, Edzell Castle Circle, Halifax, NS B3H 4J1, Canada
[c] Scottish Universities Environmental Research Centre (SUERC), East Kilbride G75 0QF, UK
[d] Earth Research Institute, University of California, Santa Barbara, CA 93106, USA

ARTICLE INFO

Article history:
Received 13 January 2012
Received in revised form
23 April 2012
Accepted 25 May 2012
Available online 27 June 2012

Keywords:
Mozambique
Lake Malawi/Niassa
Luchamange Beds
Abrupt erosion
Surface processes
Mvumu
Cosmogenic nuclide dating
Final Middle Stone Age

ABSTRACT

The late phases of the Middle Stone Age (MSA) in the East African Rift System (EARS) are known for their evolutionary shifts and association with bottlenecks, transcontinental expansion, and climatic fluctuations. The chronology of MSA sites contemporaneous with these eco-demographic upheavals is uncertain because of the scarcity of datable sites and the poor understanding of their depositional and erosional histories. We apply terrestrial cosmogenic nuclide dating in a stratigraphic section with a complex exposure history to the study of the Luchamange Beds, a widespread sedimentological unit underlying MSA sites from the shores of Lake Niassa (Mozambican EARS). We use an innovative approach, which may be applicable elsewhere, to calculate their age using a Monte Carlo-based Bayesian model that links depth profiles of 26Al and 10Be, and uses other geomorphic and cosmogenic nuclide age constraints on episodic erosion and burial. The age of the basal Luchamange Beds is 42 + 77/−15 ka, and the MSA occupation on top is 29 + 3/−11 ka. These dates suggest temporal overlap between MSA and the earliest Later Stone Age and diversity in cultural manifestations at the end of the MSA.

1. Introduction

In tropical southern Africa, the late Pleistocene is a time of marked demographic bottlenecks, population divergence, and trans-continental territorial expansion (Campbell and Tishkoff, 2008, 2010) amidst rapidly fluctuating climates and environmental deterioration (Cohen et al., 2007). The main obstacle to reconstructing Middle Stone Age (MSA) migration and cultural variation along the East African Rift System (EARS) is the lack of age constraints on archaeological assemblages. The objective of this work is to apply an innovative approach in terrestrial cosmogenic nuclide (TCN) dating to the MSA site of Mvumu. This will benchmark a relict ferruginous gravel sheet with entrained lithics that blanketed the paleolandscape of Lake Niassa/Malawi; a rift basin known for its natural passageways connecting Southern Africa with Central and East Africa (Bromage et al., 1995; Clark, 1995; Sandrock et al., 2007). The chronology for Mvumu required an innovative approach combining linked depth profiles using two different TCNs, a single nuclide depth profile in the covering alluvium, and a Monte Carlo-based Bayesian model to establish the most probable exposure history that could explain the results and quantify their uncertainty. This approach may be useful at other locations where TCN burial dating or single depth profile dating is inapplicable (e.g. Barham et al., 2011) or in places where the application of alternative dating techniques are not feasible.

2. Regional setting (Fig. 1)

2.1. The Malawi side of Lake Niassa

The MSA occupation of the southern EARS has been known for decades through surface collections and limited excavations in Malawi's Karonga district (Clark, 1966; Clark and Haynes, 1970; Kaufulu and Stern, 1987; Kaufulu, 1990; Thompson et al., in press). Unfortunately, the thousands of artifacts collected by J.D. Clark and colleagues do not associate with firm absolute dates (cf. Kaufulu and Stern, 1987; Kaufulu, 1990; Betzler and Ring, 1995).

The Malawi rift is characterized by asymmetric lake basins/shoulders (Ring and Betzler, 1995), a Proterozoic basement (Lächelt, 2004), a Phanerozoic cover called "Karoo" (Verniers et al., 1978),

* Corresponding author. Tel.: +1 403 220 5227; fax: +1 403 2829567.
E-mail address: mercader@ucalgary.ca (J. Mercader).

0277-3791/$ – see front matter © 2012 Elsevier Ltd. All rights reserved.
http://dx.doi.org/10.1016/j.quascirev.2012.05.018

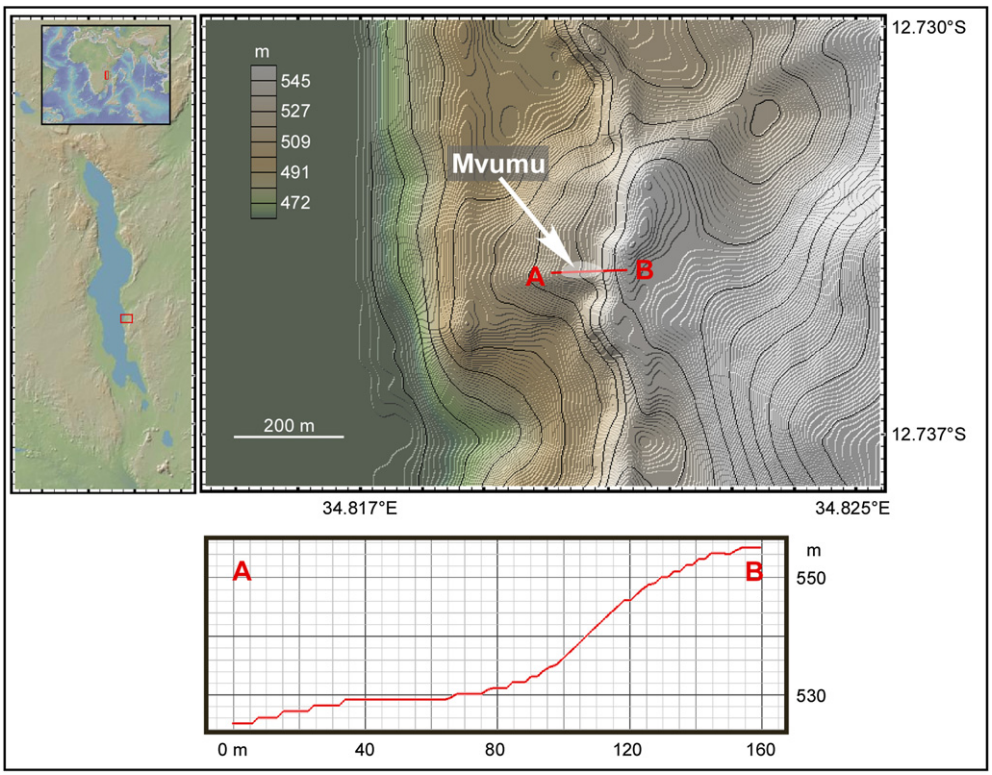

Fig. 1. Location and E–W cross section of Mvumu on the eastern shore of Lake Niassa, tropical southern Africa.

and lacustrine, fluviatile, and continental Plio-Pleistocene sediments in the uppermost part of the column (Betzler and Ring, 1995). Regional research started near Karonga at ~538 m above sea level (a.s.l.) in deposits similar to those studied here. First described by Dixey (1927) and more recently by Ring and Betzler (1995), these include the Chitimwe and Dwangwa Beds. The Chitimwe Beds lie between 500 and 800 m a.s.l. and comprise lacustrine, alluvial, colluviums, and regolith. They have been subdivided in Upper and Lower Chitimwe, together spanning several meters of thickness. Dixey (1927) described them as "discontinuous red conglomerates at the base, and a series of red gravels above" with occasional fan delta deposits. Stephens (1966) referred to them as a series of unconsolidated and cemented light red ferruginous sands and gravels forming an iron pan, and Kaufulu (1990) interpreted them as slopewash. In places, bedding is marked by discontinuous lines of small pebbles. Crossley (1986) referred to the Lower Chitimwe as clast-supported beds containing abraded stone tools and to the Upper Chitimwe as red clayey, sand-supported beds with no discernible bedding and fresh stone tools. He considered the Upper Chitimwe to be reworked by termite action (Crossley, 1986). As for the Dwangwa Beds, Dixey (1927) interpreted these as "late" lacustrine deposits that rise up to a maximum of 120 m above lake level today (~585 m a.s.l), and they were observed from Nkata Bay to Fort Maguire. The contact between Dwangwa gravels and Chitimwe sediments is an unconformity (Dixey, 1927). In Karonga, Dixey (1927) correlated the Dwangwa Beds to deposits of coarse pebbles and rock debris resting on older rocks.

2.2. The Mozambican shore

This side of the lake belongs to the rift province called "Bandawe/Metangula" featuring a half graben formed along the pre-existing "Maniamba" Karoo trough, close to a border fault system deepening to the east (Flannery and Rosendahl, 1990; Chapola and Kaphwiyo, 1992). The Metangula basin bathymetry (Ebinger et al., 1987) descends to ~290 m by the modern shore and is the extension of the Nkata/Dwangwa basins from Malawi (Specht and Rosendahl, 1987). Pinna et al. (1987) studied three formations of Neogene age. The "Mikindani" comprises Miocene and Plio-Pleistocene onshore sediments from an upper deltaic complex with red cross-stratified sands and arkoses with conglomeratic facies (Salman and Abdula, 1995; Afonso et al., 1998; Lächelt, 2004). Mid to late Pleistocene undifferentiated pediments and Holocene alluvium complete the local sequence. These pediments make up a significant part of the landscape (cf. Reid and Frostick, 1986), and they are preserved along the mountain flanks above the lake; however, their Quaternary chronologies are based on geomorphic position and weathering rather than numerical chronology or correlation with dated stratigraphy.

The lake region rises from a narrow corridor to a steep flanking mountainous range (Fig. 2). This relief configuration translates into elevation increase within a short distance eastwards, which in turn generates a climatic and botanical gradient with tropical lowland dry climates by the lake and temperate wet regimes in the highlands (da Barka and dos Santos, 2005). The lake region is covered by Zambezian woodlands which are part of the largest and most diversified African phytochorion (White, 1983; Timberlake et al., 2006).

2.3. Surficial geology (Fig. 2)

Five stratigraphic units were documented:

1) *Laterite*: A lateritic weathering profile (cf. Bettis, 2007) is widespread in the study area. It is identified by a variably altered saprolite of the uppermost <1 m to >4 m of jointed Proterozoic granitoids. The saprolite grades into a variably strained, mixed regolith and soils. Alteration decreases

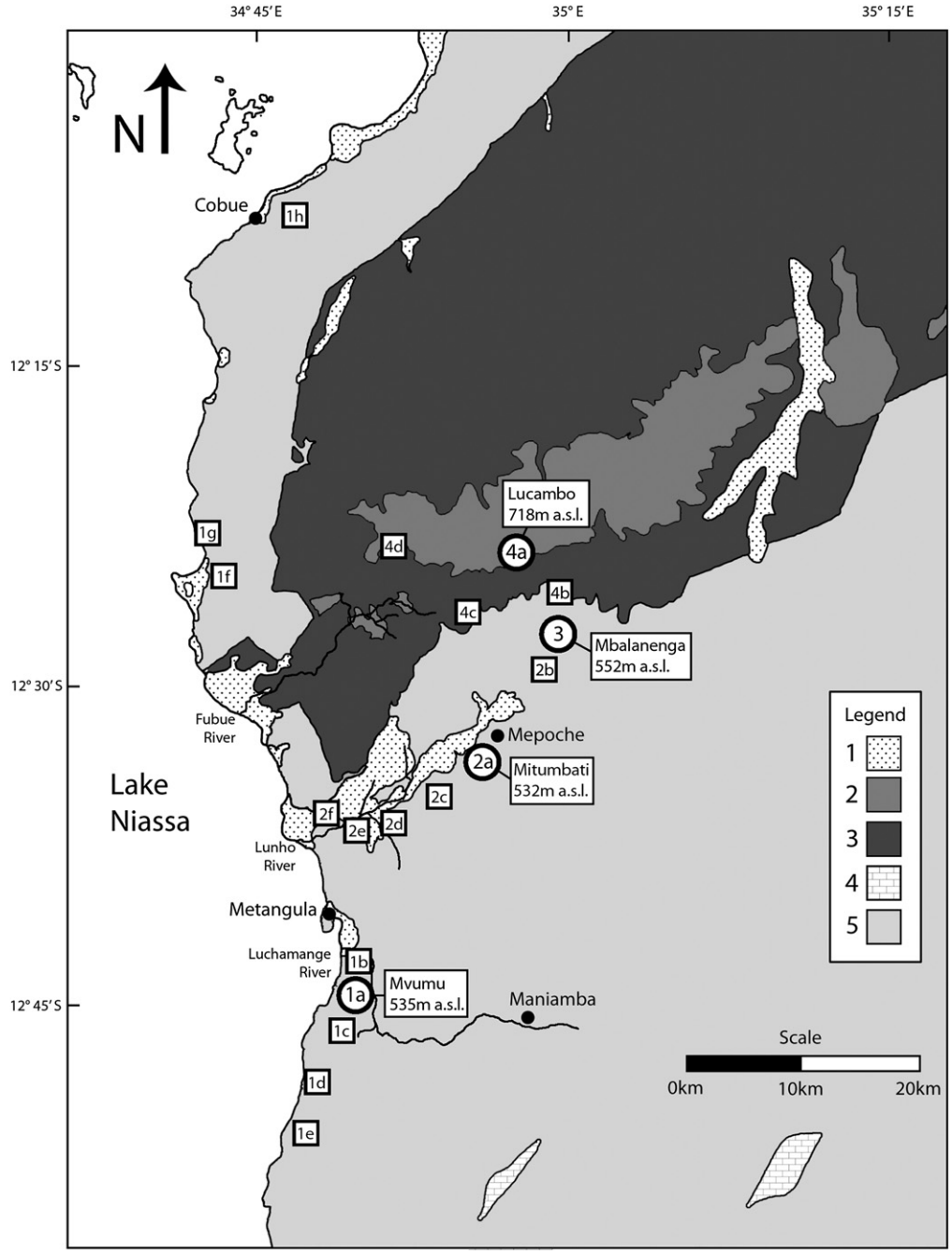

Fig. 2. Local geology and areal extent of surface survey conducted from 2003 to 2009 after Bjerkgård et al. (2007). Legend: 1) Holocene alluvium, 2) Miocene-Pliocene alluvium, lake sediment, and colluviums, 3) Phanerozoic Karoo formation, 4) Late Proterozoic dolomite, and 5) Proterozoic crystalline basement. Variably thick, undifferentiated Quaternary colluvial, alluvial, and eolian deposits (not shown on map) cover most of the Proterozoic crystalline basement. Numbered sites refer to 19 discovered and inspected loci with stratigraphies represented by four type sections (see Fig. 3).

downwards. In places, quartz and aplite veins show a diagnostic concave downward geometry, and the laterite may have its upper zone truncated and covered by allochthonous gravel. It is unclear if saprolitization is still taking place, although annual rainfall provides the flux needed for leaching. The age of this unit is unknown, but saprolites occupy a basal position and thus they are the oldest surficial materials.

2) *Colluvium*: This stratigraphic unit comprises clast- and matrix-supported diamictons and gravels emplaced by soil creep, slopewash, and debris flow. Rockslide deposits, topples, and taluses accumulate at the base of cliffs.
3) *Alluvium*: It is associated with colluvium spatially and genetically, and it seems common on gentle slopes. It is expressed as deeply incised (several meters) and gently sloped surfaces on the 30 m Digital Elevation Model (DEM) from the Shuttle Radar Topography Mission (SRTM). Raised fluvial terraces are not common because of the steepness of the terrain, but where present undoubtedly record climatic and tectonic variations in lake levels. Their age is unknown.
4) *Lake sediment*: Lacustrine clays are pervasive. Without geochemical and micropalaeontological analysis they are difficult to distinguish from Paleozoic clays. Raised shorelines

record higher lake volumes and lower rift shoulders. They imbricate with well-rounded, open-work gravels, and tend to be poorly expressed on the 30 m DEMs as their berm amplitudes are small (m-scale).

5) *Eolian deposits*. Flat benches on the order of tens of m^2 have been recorded under the woodlands covering the vicinity of Mvumu, even though they are not easily resolved on existing DEMs or topographic maps. Some eolian deposits relate to abandoned stream beds, while others could derive from lake wave-cutting, stream erosion or pedimentation. At one site, a 0.5 m thick eolian cover seems to derive from fluvial or lacustrine sands.

The maximum thickness of regional surficial sediments is ~4 m, excluding the deeper saprolite zones. No one locality exhibits all five units, although their sequences can be predicted on the basis of the relationship with slope, proximity to stream channels, and elevation above the lake. The characteristics of these units vary and artifact yielding localities in the region can be divided in four types (Figs. 2 and 3). Sites grouped under Type 1 all have coastal location and share MSA artifact-bearing units on top of the Proterozoic basement. They include Mvumu (1a), Mikuyu (1b), Malango (1c), Kolongwe (1d), Mchepa (1e), Chissomonji (1f), Nanchiwa (1g), and Cobue (1h). Type 2 spreads along the Lunho basin where Karoo siltstone is overlain by MSA-containing colluvium. Examples include Mitumbati (2a), M'fululuchi (2b), Tulo (2c), Mechumua (2d), Manheza (2e) and Daisesi (2f). Type 3 has been documented at Mbalanenga (3). Here, Karoo Formation sandstone is covered by a calcimorphic layer then capped by MSA layers. Type 4 occurs in the headwaters of the Fubue, with two instances around Lucambo (4a,b) and two in Fubue (4c) and Nacasona (4d).

The excavation at Mvumu was situated on a 20 × 20 m^2 low gradient bench on the lake's eastern shore (average 5.5°). Depth reached was 1 m to bedrock exposing four units (Figs. 4 and 5). The Luchamange Beds (named after the Luchamange basin) are at the bottom (Fig. 5, layers 4 and 3). They comprise compact clast-supported pebble grus, which in places exhibits a gradual contact with the underlying saprolite, and clast-supported, moderately sorted (granular to cobble) compact red gravels. This part of the sequence is weakly fining upward, usually with gradual contacts between weakly defined beds and a sandy matrix with >3% clay (Fig. 5, Table 1). Clasts are angular to subangular. In the section sampled for geochronology (grid E1, Fig. 6) the thickness of the Luchamange Beds to fractured bedrock is ~40–60 cm. The Luchamange Beds are thus interpreted to be a combination of colluvium, debris flow sediment, and slope wash sediment that overlie the saprolite. A shoulder bench appears to have been cut into the Luchamange Beds, with west-dipping slope of <1°. The possibility that this bench was formed by lake-wave cutting cannot be precluded. Although there is evidence of raised beaches around the lake, there is no evidence of an outlet 115 m higher than the modern one. Despite extensive field survey, another bench at a similar elevation anywhere within 20 km north or south of the site could not be found. Thus, this bench seems to be a topographic surface formed by gully incision into colluvium.

The Luchamange Beds form the majority of the cover in the vicinity of Mvumu, but at the excavation site they are unconformably overlain by archaeological deposits (Fig. 5, layer 2). Layer thickness ranges from 5 to 12 cm and clast orientation shows horizontal, inclined, and vertical positions. On top of the archaeological unit, there is a 24–44 cm thick package of upward fining grey silts and sands. They are well-sorted and weakly bedded (Fig. 5, layer 1a, b) and were deposited by alluvial fans or gully overbank (Figs. 5 and 6).

3. Materials and methods

3.1. Archaeology (SD1)

Surface survey of a transect covering 100 × 30 km and spanning 507–871 m a.s.l. (42–406 m above present-day lake level) was conducted between 2003 and 2009. Artefacts were collected from 19 localities (>10,000 lithics: Figs. 2, 7 and 8). Two sites were

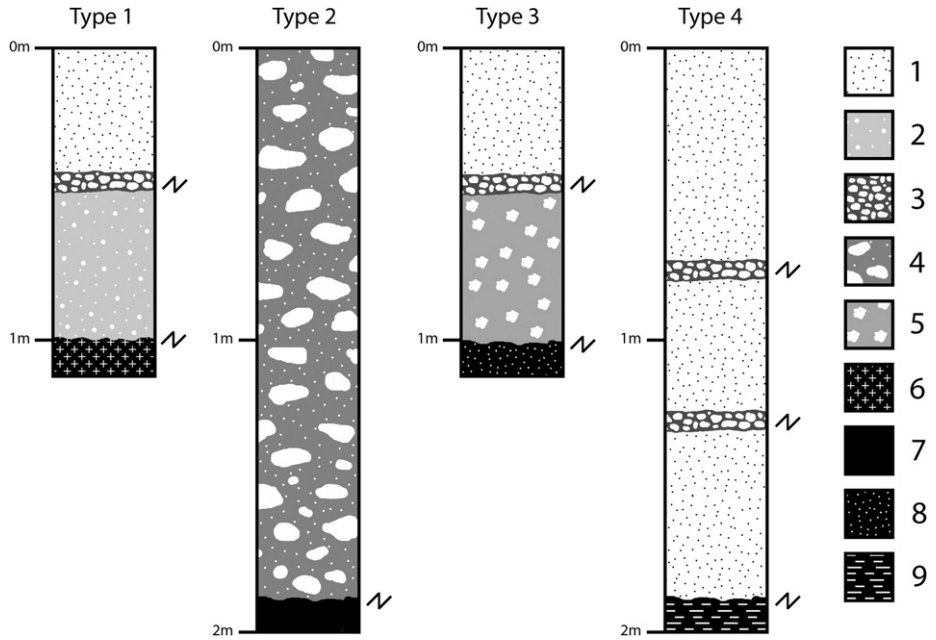

Fig. 3. Regional type profiles of surficial sediments. Legend: 1) clast-supported alluvium with possible eolian sediment, 2) variably compact pebble gravel, 3) clast-supported undifferentiated diamicton and pebble gravel, 4) coarse pebble and cobble gravel, 5) calcimorphic coarse gravel, 6) Proterozoic granitic gneiss, 7) Karoo formation siltstone, 8) Karoo formation sandstone, and 9) Mikindani formation sandstone. *N* stands for unconformity.

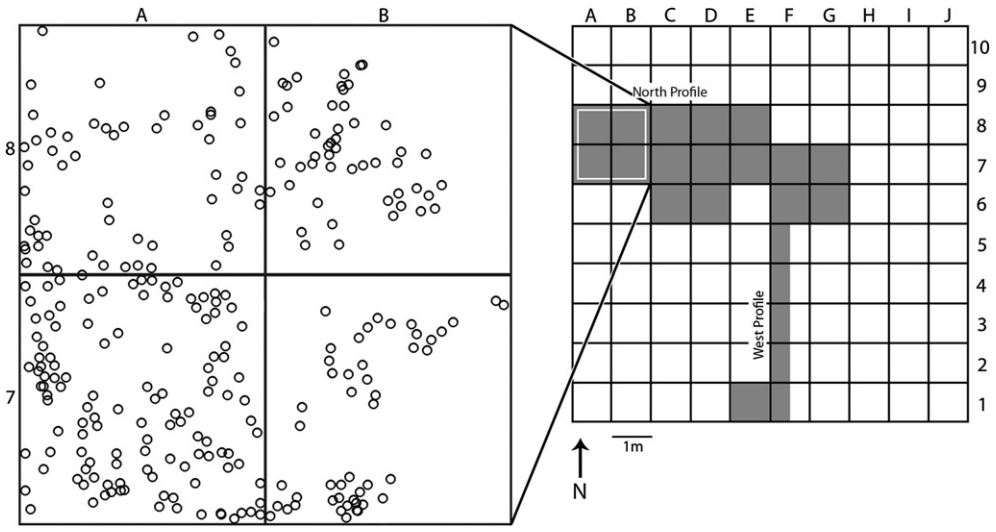

Fig. 4. Mvumu grid showing excavated areas (shaded) and horizontal lithic scatter.

selected for areal excavation: Mikuyu (Mercader et al., 2008) and Mvumu (this study). An initial series of 10 geological pits were used to guide the placement of a 10 × 10 m grid that formed the main excavation area (Fig. 4). During 2007–2008, a total of 26 m^2 were excavated within this grid with the main trench representing 19 m^2 (Fig. 4). The study assemblage was selected from 4 m^2 at the west end of the main trench (Fig. 4).

3.2. Geochronometry

Radiocarbon dating at Mvumu was impossible because of the absence of organic materials such as bone and cultural features (e.g. hearths) that would provide carbon from a closed, reliable dating context. Luminescence dating, even single grain was deemed unfeasible because of the low probability of complete bleaching of Mvumu's colluvium prior to deposition. The absence of carbonate or opaline phases made U-series dating impractical. The TCN geochronology determined the age of i) the underlying Luchamange Beds, ii) the most probable age of an abrupt erosion event that formed the bench and unconformity upon which the cultural layer lies (Fig. 6) and, iii) the age of the cap, which altogether provide maximum and minimum bracketing ages on the cultural layer in between. There was insufficient shielding from the overlying silty sands capping the archaeological remains to permit $^{26}Al/^{10}Be$ burial dating (e.g. Gibbon et al., 2009). Furthermore, the gravels appeared to have been abruptly eroded prior to burial, so a simple depth profile dating approach (Anderson et al., 1996) would not resolve a unique solution. A novel approach that simultaneously used depth profiles of two different TCN measured in the same samples allowed us to consider the complexity of an exposure history with multi-stage deposition and sudden, incremental erosion.

Sixteen 3 kg samples of amalgamated sands and sandy pebble gravel were collected for depth profile dating using ^{10}Be and ^{26}Al (Anderson et al., 1996; Hidy et al., 2010, Table 2). Fourteen of the samples were collected from ~3 cm thick zones at different depths in both the Luchamange Beds and the overlying silty sands (Fig. 6).

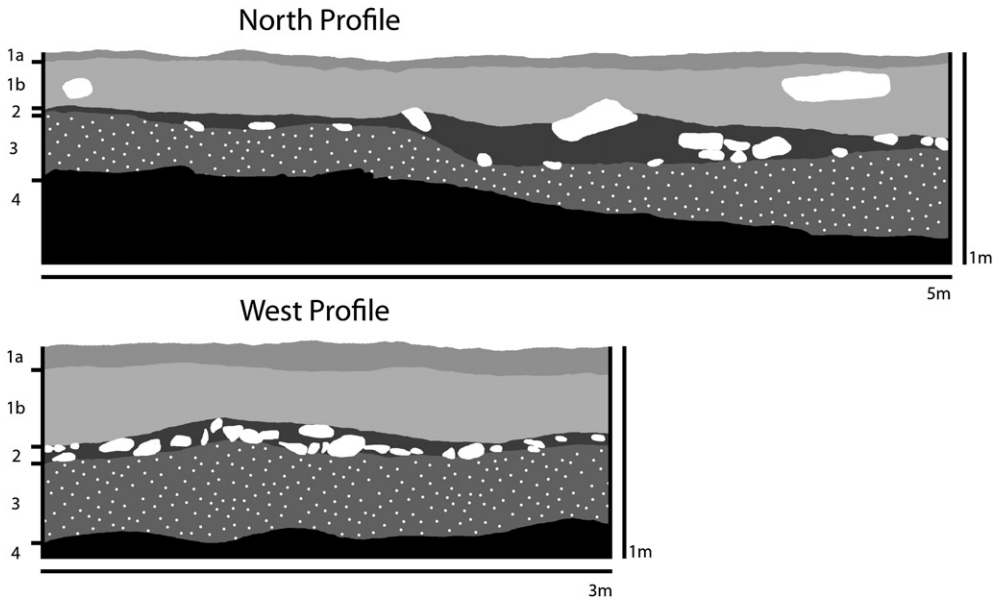

Fig. 5. North and west profiles at the site of Mvumu (compiled from the transects 8/9 and 7/8 for the north profile, and transect E/F for the west profile, refer to Fig. 4). Layer numbering is on the left side. Layer 2 represents the MSA occupation of the site where most lithics were found.

Table 1
Color, pH, organic carbon content, water, and particle size of sediments from Mvumu. Column sampling carried out in the north profile of grid C1 (Fig. 4).

Sample	Depth, m	Color (field)	pH	Organic carbon %	Water %	Sedimentology	Mean particle size, microns	Sand %	Silt %	Clay %
X	0.005–0.02	10YR 3/2 (very dark grayish brown)	6.53	6.35	1.71	Silty sand	125	74	24	2
IX	0.05–0.08	10YR 4/3 (brown)	6.22	3.69	1.87	Silty sand	207	71	21	8
VIII	0.16–0.19	10YR 4/6 (dark yellowish brown)	6.29	4.67	2.38	Silty sand	73	72	25	3
VII	0.30–0.32	10YR 4/6 (dark yellowish brown)	6.16	4.95	1.68	Silty sand	200	72	25	3
VI	0.37–0.040	7.5YR 4/6 (strong brown)	6.23	3.07	1.91	Silty sand	123	70	26	4
V	0.45–0.48	7.5YR 4/6 (strong brown)	6.28	4.34	2.56	Silty sand	223	59	27	14
IV	0.61–0.64	7.5YR 4/6 (strong brown)	6.4	6.15	3.23	Silty sand	44	64	32	4
III	0.70–0.73	7.5YR 4/6 (strong brown)	6.38	14.81	2.13	Silty sand	143	65	32	3
II	0.82–0.86	7.5YR 4/6 (strong brown)	6.45	6.18	3.71	Silty sand	279	70	18	12
I	0.92–0.95	7.5YR 4/6 (strong brown)	6.24	5.47	3.73	Silty sand	189	63	34	3

In addition to those, we collected two swath samples that ranged over most of the 40-cm Luchamange and 33-cm capping alluvium (Fig. 6). The swaths provide a useful check on the total average ^{10}Be concentration for the section and insights into the timing and extent of sediment mixing (cf. Perg et al., 2001). Additionally, bulk density samples (Fig. 6) of approximately 1 kg were collected in both the Luchamange Beds and capping alluvium in order to estimate the bulk density in those layers. Details of the physical and chemical preparation of the Al_20_3 and BeO targets for accelerator mass spectrometry (AMS; Rood et al., 2010), blank corrections, standards, and uncertainty in the ^{10}Be and ^{26}Al concentration are provided in the supplementary data file SD2. For consistency among the samples, we used the 250–355 μm size fraction sieved from each sample. It was the coarsest fraction with sufficient mass for the chemistry, and we were concerned that the finer grained sediment may have a different exposure history (Belmont et al., 2007; eolian deposits were observed in the region) and thus may contribute a different inherited concentration. A duplicate sample was analysed on the 150–250 μm fraction in one sample to test the sensitivity of grain size on concentration.

3.2.1. Model 1. One stage deposition-exposure

The ^{26}Al and ^{10}Be concentrations from the Luchamange Beds profiles and the overlying sands were interpreted first as simple exposure ages using the Matlab™ age calculator code of Hidy et al. (2010) vers. 1.2. In these simplified calculations the fact that there may have been an unconformity of unknown duration, and a subsequent cover of alluvium were ignored. The measured bulk densities of 1.8 ± 0.1 g cm^{-3} and 2.2 ± 0.1 g cm^{-3} for the capping sands and Luchamange Beds respectively, were used to constrain an integrated bulk density with depth profile for the model. All site production rates are based on Stone (2000) after Lal (1991) as per Balco et al. (2008), and corrected for a 2% (minimum) shielding of the cosmic ray flux by a variable vegetation cover (Plug et al., 2007). The results were not adjusted for possible influences on production rate of variations in the geomagnetic field (adjusted age would be 7% less: averaging all scaling methods, but a maximum decrease of 11% is obtained using Lifton et al. (2005) scaling model; Balco et al., 2008) or atmospheric changes (<1% effect; Staiger et al., 2007). Muon production rates with depth were approximated with a five term exponential fit to the theoretical values of Heisinger et al. (2002a,b) as modified by Balco et al. (2008). A maximum of 30 cm of gradual erosion of the Luchamange Beds prior to the abrupt event was assumed. To test this assumption, the slope average erosion rate (0.004 cm a^{-1}) was estimated by using the inheritance value measured in both the ^{26}Al and ^{10}Be depth profiles as a surrogate for paleo-sediment flux rate (e.g. Charreau et al., 2011), and then multiplied this by the calculated exposure age of the Luchamange Beds (see below).

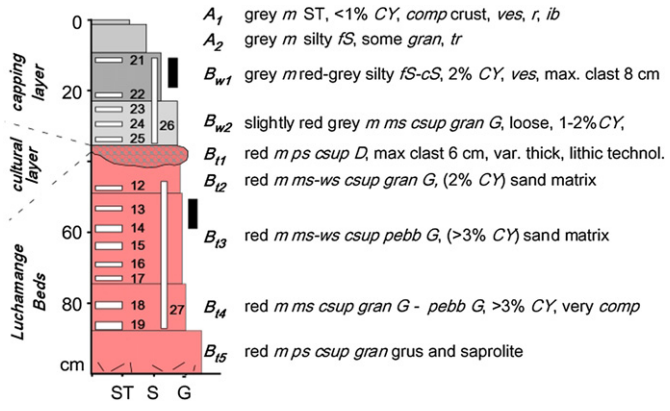

Fig. 6. Simplified, composite column at Mvumu: stratigraphy and soil horizons. Upper 37 cm from grid G7, remaining from cell E1. Numbered white boxes indicate thickness and position of TCN samples, including swath samples 26 and 27. Black boxes show location of bulk density samples. *comp*: compact, *cS*: coarse sand, *csup*: clast supported, *CY*: clay, *D*: diamicton *fS*: fine sand, *G*: gravel, *gr*: grass roots, *gran*: granular, *ib*, insect burrows, *m*: massive, *msup*: matrix supported, *ms*: moderately sorted, *pebb*: pebbly, *ps*: poorly sorted, *ST*: silt, *S*: sand, *tr*: tree roots, *ves*: vesicular, *ws*: well sorted.

The Hidy et al. (2010) calculator uses a Bayesian Monte Carlo approach to model ages for ^{26}Al or ^{10}Be measurements in a depth profile and permits the incorporation of site-specific geologic data (e.g. variable bulk density with depth) and inferred boundary conditions (e.g. limits on total surface erosion and erosion rates) into the calculation. Returned Bayesian most probable ages and uncertainties are acquired from relative probability density functions constructed from the age results of all solutions generated from a customized Monte Carlo simulation. Additionally, age distributions within user-defined confidence windows (1σ, 2σ, etc.) are returned to assess not just the most probable result, but at what confidence level the profile data adhere to a theoretical depth profile (implemented with a chi-squared statistic). For the case of simple exposure ages from depth profiles, 1 million simulated profiles fit within a 2σ range of the individual measured ^{10}Be concentrations; for ^{26}Al, 100,000 profiles fit within the 3σ range. The two- and three-sigma ranges include the measured AMS precision and an additional uncertainty associated with chemistry and ICP error; bulk densities were assigned a 0.1 g cm^{-3} uncertainty. Although the total error in age exceeds the ~10% uncertainty assigned for production rate error (Balco et al., 2008), these calculations do not account for the complexity in the local depositional and erosional history and so underestimate the true error in age.

3.2.2. Model 2. Multi-stage deposition-exposure

Recognizing that the Luchamange Beds were not always exposed at their current depth and were likely affected by an abrupt erosion event prior to burial, a more elaborate calculation was necessary. By using the capping sands depth profile, estimates of

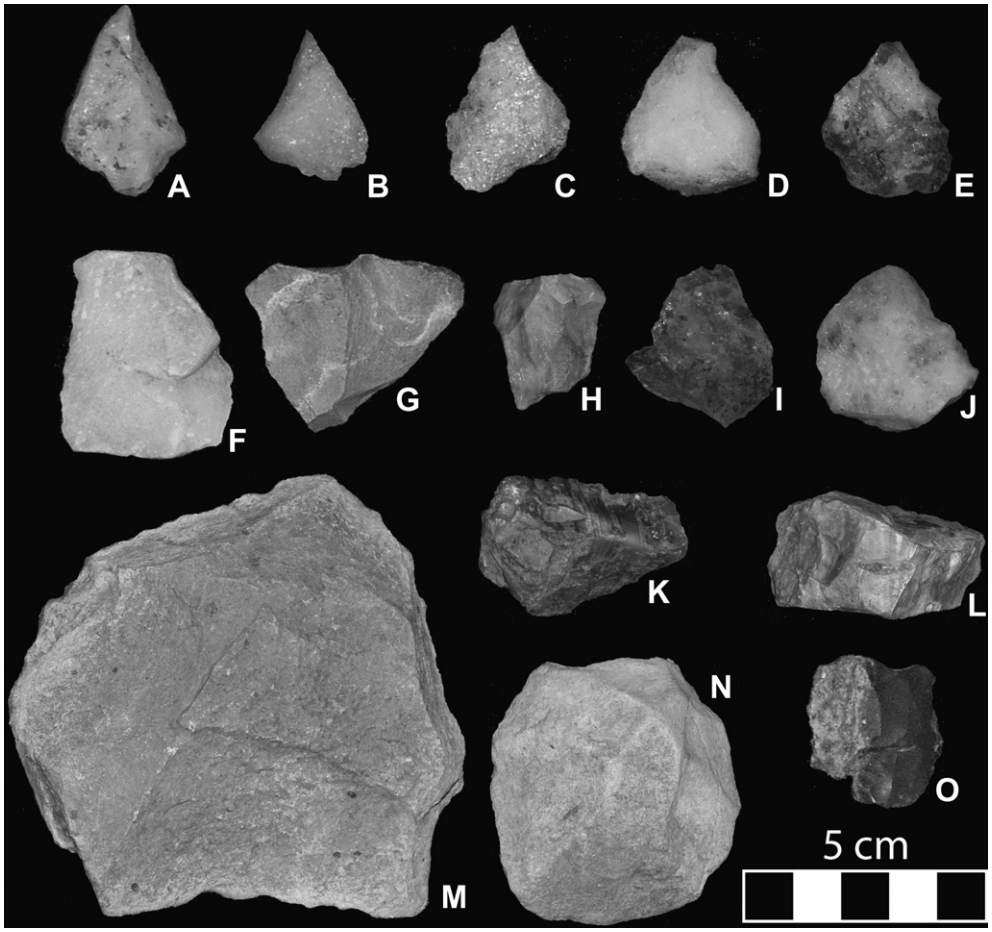

Fig. 7. Selected sample of Middle Stone Age lithics collected during regional surface survey (Fig. 2): a) Quartz shouldered point from M'fululuchi b, c, d) Quartz awls from Daisesi e) Quartz awl from Mitumbati f) Quartzite side scraper from Mitumbati g) Rhyolite core fragment from Mitumbati h) Chert core fragment from Mitumbati i) Crystal quartz flake fragment from Mitumbati j) Quartz flake scraper from Mitumbati k, l) Chert core fragments from Mitumbati m) Large rhyolite scraper on flake from Mitumbati n) Rhyolite discoidal core from Mitumbati o) Chert flake fragment from Mitumbati.

net erosion into the slope, and simultaneously using the ^{10}Be and ^{26}Al concentrations, the chronological objectives were met. Model 2 utilizes modified Matlab™ code from Hidy et al. (2010) vers. 1.2 to include two features that were unavailable in Model 1: 1) discrete abrupt erosion and aggradation, including intermittent episodes of gradual erosion/aggradation, and 2) simultaneous simulation of ^{26}Al and ^{10}Be profiles to yield a combined most probable result from both profiles. In order to increase the likelihood of obtaining probable solutions, an arbitrarily large chi-squared cut-off of 100 was imposed to remove solutions with effectively zero probability. The chi-squared statistic was then converted to a probability using the chi-squared likelihood function and applied to the set of parameters that created it. Details of the Monte Carlo-based Bayesian controlled computation in Model 2 are provided in the supplementary file SD3 along with access to the full code (SD4) and output based on 1 million simulations (SD5).

Specifically, the site at Mvumu presents us with four stratigraphic events that require absolute dating with Model 2 (see SD4 and SD5). **Event 1**—deposition of the Luchamange Beds occurred at an unconstrained time and the paleo surface of the Luchamange Beds was allowed to erode continuously at a random value between −1.0 and 4.5 cm/ka based on the depth profile constraints (negative erosion permits the possibility of aggradation at the sample site). Unconstrained values of inherited ^{10}Be and ^{26}Al were randomly chosen but assumed constant with depth at time of deposition. **Event 2**—an incremental erosion event with a randomly chosen magnitude between 90 and 150 cm occurred at an unconstrained time after Luchamange Bed deposition, but before deposition of the overlying cultural layer (Figs. 5 and 6; calculation of erosion thickness is described below). **Event 3**—an unconstrained period of relative stability between the incremental erosion event. This step includes a short occupancy time of the site and deposition of the stone technology directly and indirectly through slope washed colluvium from upslope. The short occupancy time does not influence the modelled ages. **Event 4**—deposition of the overlying alluvium constrained by the upper depth profile age with an erosion rate varying between 0 and 0.5 cm/ka.

4. Results

4.1. Archaeology

Based on surface lithic scatters Mvumu covers ~10 ha over a roughly oval area (Fig. 1) (E–W axis: 500 m, N–S axis: 200 m) at 65–115 m above present-day lake level (530–580 m a.s.l.). The highest artifactual density occurs at S 12° 44.099′/E 34° 49.149′ ± 5 m. Straight-line distance to the lake is ~200 m. Angular to subrounded pebble to cobble-sized pegmatitic quartz blankets the hill, with increasing numbers near the site's summit. The stone tools presented here total 1977 (Bennett, 2011). The raw materials are milky quartz (94.1%), quartzite (4.5%), quartz crystal (1.2%), rhyolite (0.2%), and chalcedony (0.1%). Three quarters of the quartz

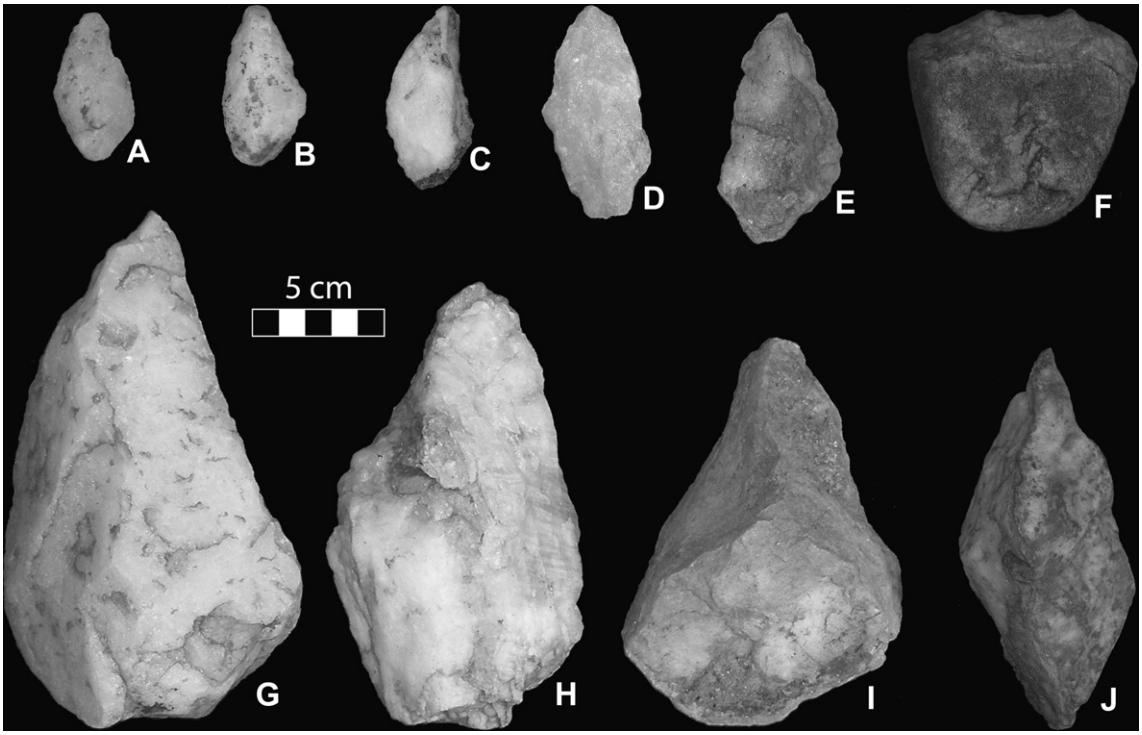

Fig. 8. Middle Stone Age surface lithics from Mikuyu; a site adjacent to Mvumu and part of the same geological formation (Locus 1b in Fig. 2): a–e) Quartz bifacial pieces f) Pebble scraper, quartzite g–j) Core axes in quartz.

exploited is a fine-textured, light grey (10YR 7/1) type, while the rest is coarse-textured, white (2.5Y 8/1; 10YR 8/1) milky quartz. The lithic assemblage is made up of debitage (83%), formal tools (11%), and cores (6%). A significant proportion of the assemblage (96%) is in fresh condition, with rare instances of slightly weathered pieces (4%) and no examples of heavy weathering. Retouch, the removal of small flakes from the blank edges to intentionally modify its initial shape, affects 10% of the total assemblage. Core types appear in Table 3 and Fig. 9. Non-prepared cores (63%) are expedient cores that do not follow pre-established reduction templates. Platform, polyhedral cores (Clark and Brown, 2001:317) display the greatest metric range (mean length: 50 mm). Although some specimens may be extensively used, the majority are underexploited; number of flakes removed is four. Residual platform angles average 82° but 25% of the simple cores shows angles >90°. Prepared core technologies (37%) are those in which the artisan removes flakes from the core to obtain a desired size and shape, which at Mvumu run in second place. Slightly less than half of these prepared core technologies are discoidal *sensu stricto* (e.g. Clark and Kleindienst, 2001), while the remainder is Levallois *sensu lato* (Clark and

Table 2
Geological and geochemical data for the cosmogenic ^{10}Be and ^{26}Al measurements. Lat: S 12° 44.099′, Long: E 34° 49.149′, Elev: 527 m.

Sample ID	Unit	Pit	Depth to top (cm)	Thickness (cm)	Soil horizon	^{10}Be conc ×1000 (atom/g)	^{10}Be error ×1000 (atom/g)	^{26}Al conc ×1000 (atom/g)	^{26}Al error ×1000 (atom/g)	^{26}Al/^{10}Be
MOZ-08-MV-TCN-12	Luchamange	E1 north face	47	2	Bt2	134.3	3.3	921.2	26.1	6.86
MOZ-08-MV-TCN-13	Luchamange	E1 north face	53	2	Bt3	135.1	3.1	812.5	17.6	6.01
MOZ-08-MV-TCN-14	Luchamange	E1 north face	57	3	Bt3	115.5	2.6	649.2	22.3	5.62
MOZ-08-MV-TCN-15	Luchamange	E1 north face	63	2.5	Bt3	106.9	2.6	633.1	15.2	5.92
MOZ-08-MV-TCN-16	Luchamange	E1 north face	68	3	Bt3	101.4	2.3	621.6	16.4	6.13
MOZ-08-MV-TCN-17	Luchamange	E1 north face	73.5	2	Bt3/Bt4	88.5	2.0	563.4	35.5	6.37
MOZ-08-MV-TCN-18	Luchamange	E1 north face	79	3	Bt4	111.4	22.3	546.3	19.9	4.90
MOZ-08-MV-TCN-19	Luchamange	E1 north face	83.5	3.5	Bt4	82.6	1.9	445.8	17.2	5.40
MOZ-08-TCN-12-250um	Luchamange	E1 north face	47	2	Bt2	171.0	3.2	1041	33.0	6.09
MOZ-08-MV-TCN-27	Luchamange-swath	E1 north face	45	43	Bt3	110.3	2.6	–	–	
MOZ-08-MV-TCN-21	Capping Sands	H8 west face	11	2	SL Bt1	174.9	4.0	–	–	
MOZ-08-MV-TCN-22	Capping Sands	H8 west face	20	3	SL Bt1	174.4	4.0	–	–	
MOZ-08-MV-TCN-23	Capping Sands	H8 west face	27	3.5	Bt2	163.0	3.7	–	–	
MOZ-08-MV-TCN-24	Capping Sands	H8 west face	33	3	Bt3	163.8	3.9	–	–	
MOZ-08-MV-TCN-25	Capping Sands	H8 west face	38	4.5	Bt3	177.2	4.0	–	–	
MOZ-08-MV-TCN-26	Capping Sands-swath	H8 west face	10	33	Bt3	177.1	2.8	–	–	

Notes: Site is 12° 44.099′ S/34° 49.149′E ± 5 m from GPS; 530 m ± 30 m from GPS; 07KNSTD with ^{10}Be/^{9}Be ratio of 2.85×10^{-12} (Nishiizumi et al., 2007) and KNSTD with ^{26}Al/^{27}Al of 1.065×10^{-11} (Nishiizumi, 2004); blank correction in at/g and % of total; Errors are 1-sigma AMS uncertainties only.

Table 3
Lithic Core types from Mvumu: grids A7, A8, B7, and B8.

Core type	*n*	%
Simple	61	47.66
Discoidal	19	14.84
Preferential discoidal – recurrent	9	7.03
Levallois-like	8	6.25
Elongated high backed core	7	5.47
Low backed unifacial radial	6	4.69
Preferential discoidal – single	6	4.69
Elongated high backed on flake	5	3.91
Testing	4	3.13
Bipolar	3	2.34

Kleindienst, 2001). Mean length is 47 mm (range: 33–77 mm). Average platform angle for discoidal cores is 72°, and a typical core has nine flakes removed from it (range: 6–13). "Preferential" discoidal cores can be recurrent or single (see Mercader et al., 2009), which are essentially Levallois types except for the fact that the non-preferential side of the core still yields blanks of usable size. Mean maximum length is 55 mm and 48 mm, and their mean mass is 58/47 g respectively. The mean number of removals from both types is seven. Platform mean angle is 66°. Levallois cores (*sensu lato*) reach a mean maximum size around 45 mm and mean mass of 23 g. Striking platform angles average 86°. Lastly, bipolar technology as defined by Clark and Kleindienst (2001:61) is extremely rare (Mercader et al., 2008, 2009): Mvumu's bipolar cores amount to 2%. Specialized blade cores (Inizan et al., 1999) are absent.

Debitage (Table 4) is divided into two groups: <1–20 mm (52%) and ≥20 mm (48%). The total number of whole flakes is 721 (mean maximum length = 20.8 mm, width = 19.7 mm, thickness = 6.7 mm, mean mass = 3.6 g). A majority of flakes are longer than they are wide ("under-square" types: 56.2%), while others are "over-square" (wider than they are long: 43.8%). A small portion of elongated flakes (<1% of the total number of flakes) resemble blade-like products, but given the lack of blade cores, these pieces are not considered to be formal blades. Cortex appears as stream worn or physicochemically weathered surfaces. Cortical representation by size category increases with larger size pieces, so that 1–20 mm fragments represent 40% of the cortical pieces ($n = 94$) and lithics >20 mm peak at 60% ($n = 145$). Cortical platforms are 5% of the total. The mean width of non-cortical platforms is 12.3 mm, with a thickness of 5 mm, and an external angle of 75°. Platform preparation, however, is uncommon, with 85.7% of our flakes displaying no faceting and 11.8% showing two facets only, while three and four-faceted specimens combined represent 2.5% of the assemblage. The dorsal patterns of extraction is irregular (95.6%), with parallel extractions represented in 3% of the specimens and radial on a 1.4%. Termination types include feather (72%), step (10.6%), concave step (*sensu* Isaac, 1977) (10.2%), hinge (5.2%), and overshot (2%).

Over half of the tools (58%) are made on flakes, while 42% were core-based. Formal tools group in four categories (Fig. 10, Table 5): scrapers (53.8%), awls (14.5%), points (7%) and miscellaneous tools (24.7%). Unifacial retouch dominates (87.5%) and is typically confined to the tool's edge. However, not every tool is retouched. Bifacial retouch is absent. Scrapers can be subdivided in several subtypes (Fig. 10, Table 5), and most of them were produced on flake blanks (65%). The most common type is the convex scraper. Most are made of fine milky quartz with a retouched, convex edge and average 45 mm in maximum length and weigh 20 g. The convex edge scraper represents 20% of the total tool inventory. The second most prominent scraper type is called "bevel-based" (Fig. 10, Table 5) (cf. Clark and Kleindienst, 2001), which amounts to 12% of all formal tools, with a mean maximum length 46 mm and mass of 27 g. The third most abundant scraper type is the core scraper (8%)

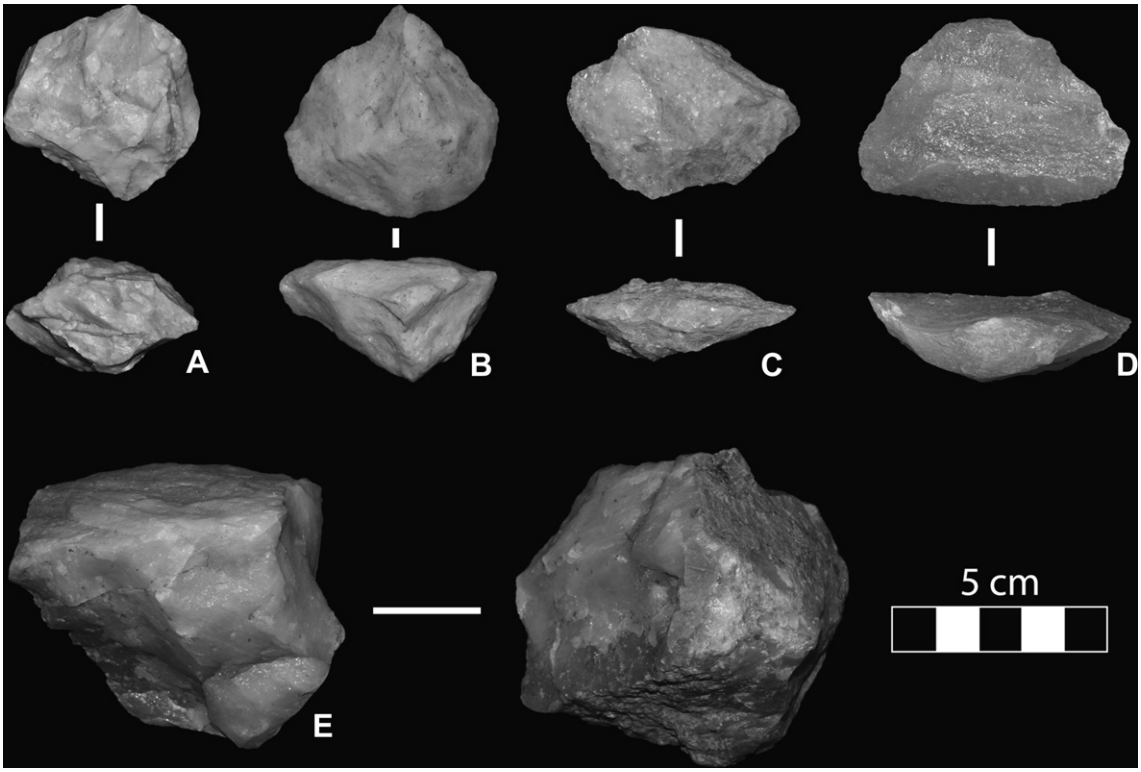

Fig. 9. Selection of core types from the Mvumu excavation: a) Discoidal core, grid B7 b) Recurrent preferential discoidal core, grid B7 c) Single preferential discoidal core, grid B8 d) Levallois core, grid B8 e) Polyhedral core, grid B7.

Table 4
Lithic debitage from Mvumu: grids A7, A8, B7, and B8.

Debitage	*n*	%
Whole flake	721	44.10
Shatter	417	25.50
Proximal flake fragment	173	10.58
Distal flake fragment	140	8.56
Medial flake fragment	108	6.61
Core trimming element	47	2.87
Elongated flake	7	0.43
Proximal truncated flake	7	0.43
Lateral truncated flake	6	0.37
Core tablet	4	0.24
Distal truncated flake	4	0.24
Hammerstone fragment	1	0.06

(Fig. 10, Table 5). They measure 56 mm and weigh 61 g on average. Awls were made by a truncation technique where one end of the blank is rested on an anvil and struck with a perpendicular blow while the other end is raised slightly (cf. Moore et al., 2009) (Fig. 10, Table 5). This is a departure from the traditional interpretation of these tools where they are considered to be made by burination (e.g. Barham, 2000). One third of the points from the lake region (see also Mercader et al., 2008, 2009) are corner struck (cf. Armstrong, 1931; Brooks et al., 2006). Another point type is "Levallois-like" ($n = 3$), some of which have incipient tangs. Unifacially retouched, based-struck pointed flakes are documented twice. All point types combined ($n = 15$), except for one outlier, measure 30 mm in maximum length (range = 20–41 mm) and have an average mass of 25 g. The exception is one point 64 mm long that weighs 44 g. Microliths are superficially similar to blade-based "geometrics" ($n = 10$) but they are made on nondescript blanks.

4.2. Geochronometry

4.2.1. Model 1. Single stage deposition and exposure

The concentration versus depth profiles for the Luchamange Beds (AMS precisions averaged 2% for ^{10}Be and 3% for ^{26}Al; Fig. 11) yield Bayesian most probable ages of $47.8^{+7.0}/_{-11.6}$ ka (2σ total error) and $46.7^{+6.3}/_{-6.9}$ ka for ^{10}Be ($n = 6$) and ^{26}Al ($n = 7$) (Fig. 12; Table 2, SD3). The characteristic exponential shape of the profiles verifies that there has been negligible post-depositional mixing of the Luchamange Beds below the cultural layer (Fig. 6). The small but visible scatter in the concentrations of both ^{10}Be and ^{26}Al profiles (Fig. 11) suggests that either the beds were not deposited together, the beds have slightly different inheritance concentrations, or both. For the Luchamange Beds, the estimated inheritance concentrations for ^{10}Be and ^{26}Al overlap, and their 'Bayesian most probable' and modal values are very low, 5200 $^{+31,900}/_{-900}$ and 0 $^{+113,200}/_{-0}$ atoms g^{-1} respectively, indicating that most of the concentration was produced in situ (Table SD3). A slightly higher ^{10}Be inherited component is also consistent with the relatively ^{26}Al/^{10}Be measured and may indicate partial burial of the colluvial gravel prior to deposition at Mvumu. We note that TCN-14 and TCN-13 were omitted from the respective depth profiles. We have included the original data for these samples (SD2) however we are unable to obtain 2σ fits for either ^{26}Al or ^{10}Be curves if they are included. Possible reasons for their error may be any combination of (i) inconsistent inheritance with depth in a colluvial gravel; (ii)

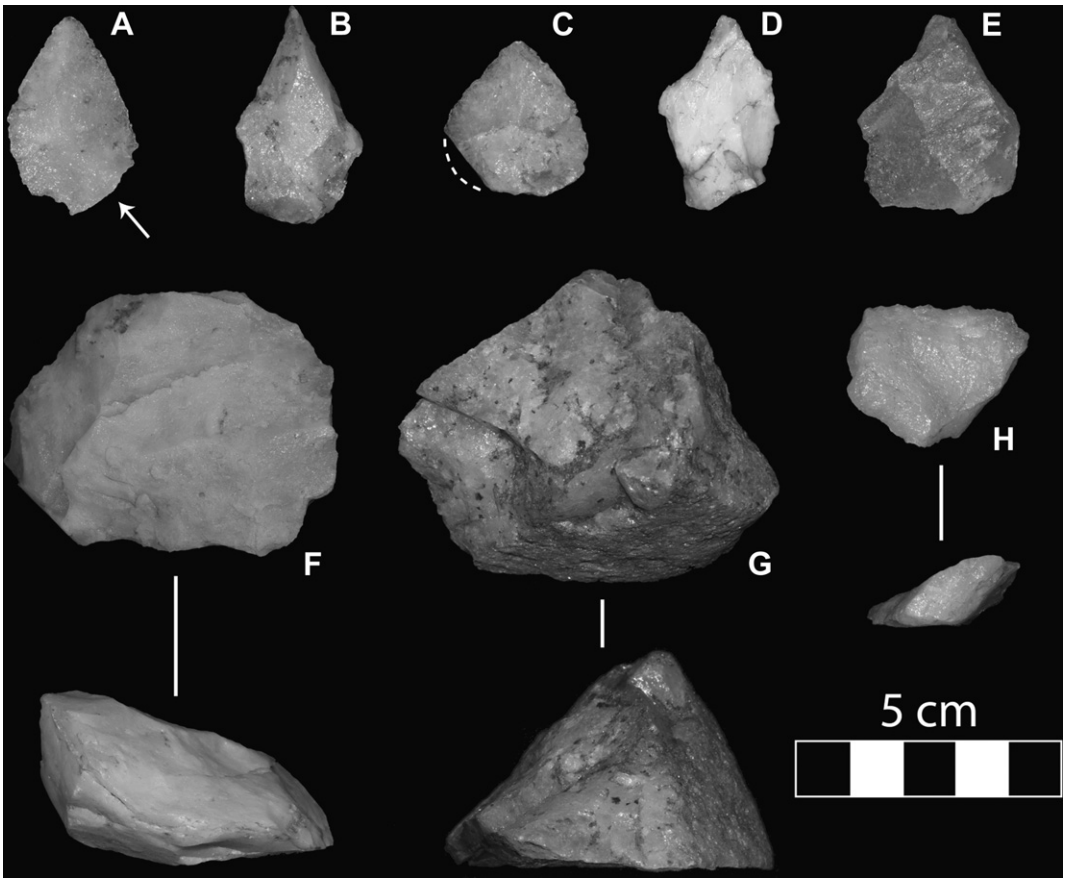

Fig. 10. Quartz lithics from Mvumu. Excavation: a) Corner-struck point, grid A7 b) Levallois point, grid A7 c) Base-struck point, grid B8 d) Single truncation awl, grid B7 e) Double truncation awl, grid A8 f) Convex scraper, grid B8 g) Core scraper, grid A8 h) Bevel-based scraper on flake, grid B8.

Table 5
Stone tool classification from the excavated materials from Mvumu: grids A7, A8, B7, and B8.

Tool	*n*	Flake blank	Core blank
Scraper, bevel-based	24	7	17
Scraper, convex side	24	10	14
Scraper, convex end	17	7	10
Scraper, core	16	0	16
Scraper, semi-circular	10	4	6
Scraper, concave	6	2	4
Scraper, convergent	6	3	3
Scraper, denticulate	3	2	1
Scraper/Awl	3	2	1
Scraper, denticulate semi-circular	2	2	0
Scraper, end and side	2	2	0
Scraper, convex-concave	1	0	1
Scraper, denticulate core	1	0	1
Awl, single truncation	18	12	6
Awl, double truncation	8	8	0
Awl, topknot	3	3	0
Awl, double retouched	1	1	0
Awl, triple truncation	1	1	0
Point, corner-struck	10	10	0
Point, base-struck	2	2	0
Point, Levallois-like – shouldered/tanged	2	2	0
Point, Levallois-like – simple base	1	1	0
Retouched piece	23	19	4
Pointed piece	11	10	1
Retouched/prepared snapped piece	8	8	0
Notch	3	3	0
Pebble tool	3	0	3
Crescent	2	2	0

unrecognized bioturbation; and (iii) unrecognized error in chemistry or AMS. Their omission does not significantly affect the ages obtained (<5% difference with the modal age at if all data were included at 5σ).

Although the two ages are in very close agreement and it is tempting to accept them as the age of the Luchamange Beds, the observed stratigraphic and geomorphic relationships preclude the validity of this simple interpretation because the abrupt erosion event and delayed burial by the capping sands has not been considered. To date the capping fluvial sand, the same grain size fraction of quartz that was used to date the Luchamange Beds was employed. The concentrations of the five ^{10}Be samples in the capping fluvial sand unit are very similar (coefficient of variation about the mean of 3.9%, Table 2). Their uniform concentration with depth indicates either that the sediments have recently experienced a very rapid erosion rate, or that the sediments are very young. As there is no geomorphic or soils evidence for rapid erosion at the surface of the site or in the depth profile of the underlying Luchamange Beds, and considering the weakly developed soil in the alluvial sands (weak B horizons, Fig. 6), this paper favors the latter interpretation. The Bayesian most probable age of the depth profile for Model 1 (assuming bulk density is 1.8 ± 0.1 g cm^{-3}, erosion rate of 0–0.0009 cm a^{-1}, that limits total erosion to 30 cm based on negligible tree root exposure and general lack of evidence of erosion and an unconstrained inheritance, using 100,000 simulations) is $5.7^{+14.7}/_{-5.1}$ ka (2σ). It is noteworthy that the Bayesian most probable inheritance concentration for the capping sands is 155,000 atoms g^{-1}, much larger than the inheritance in the Luchamange Beds, but consistent with the top of the Luchamange Beds being the source of the sands. Subtracting the equivalent of 5.7 ka of ^{10}Be from the ^{10}Be concentration measured in the uppermost sample in the Luchamange Beds (Table 2) yields 108,000 atoms g^{-1} in the source quartz. This is a minimum constraint on the inheritance concentration of the Luchamange Beds upslope from the site because at the sampling location the Luchamange Beds were eroded. An immediate source of the

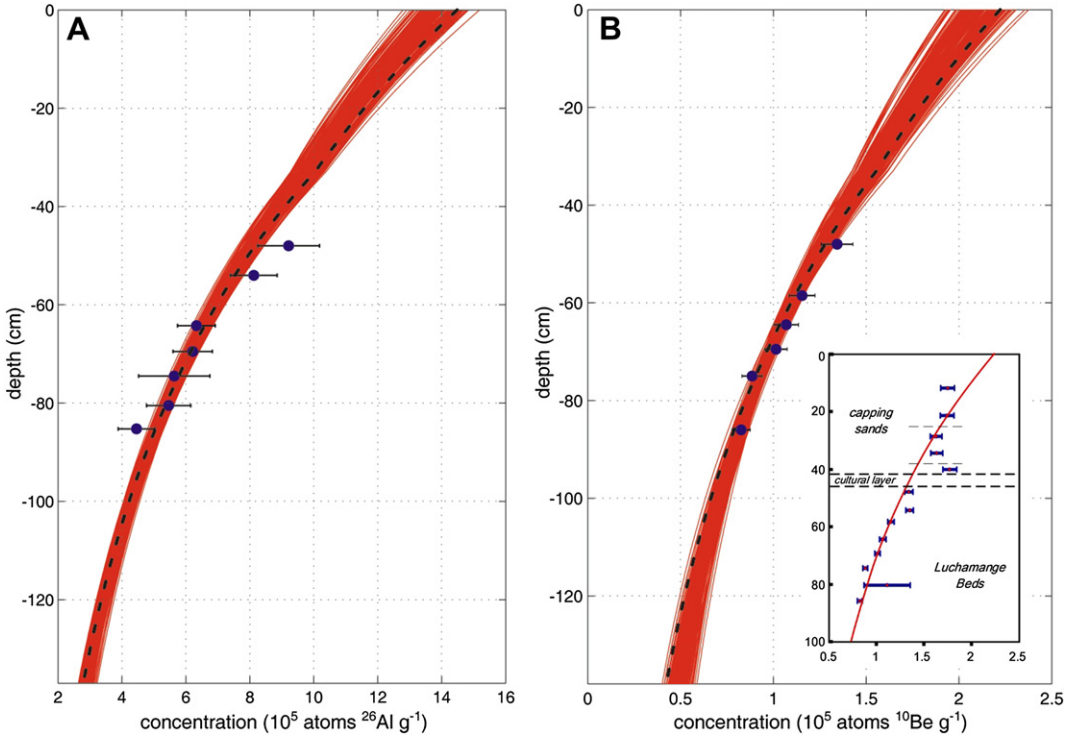

Fig. 11. Model 1 concentration versus depth profiles for the Luchamange Beds samples. A. ^{26}Al. Dashed black curve represents the age-erosion-inheritance scenario with the lowest chi-square fit of the data. Family of red curves are all 100,000 curves fitting within the 3σ error of each measured concentration. Bulk density and sample characteristics provide in the text and Fig. 6. B. ^{10}Be. As above, except 1,000,000 curves at 2σ error. Inset: depicts the concentrations of all 10Be measurements. Horizontal dashed lines indicate stratigraphic or soils boundaries as described in the text. Error bars are 1s AMS precision. Red curve is lowest chi-square fit of 1000 curves. (For interpretation of the references to color in this figure legend, the reader is referred to the web version of this article.)

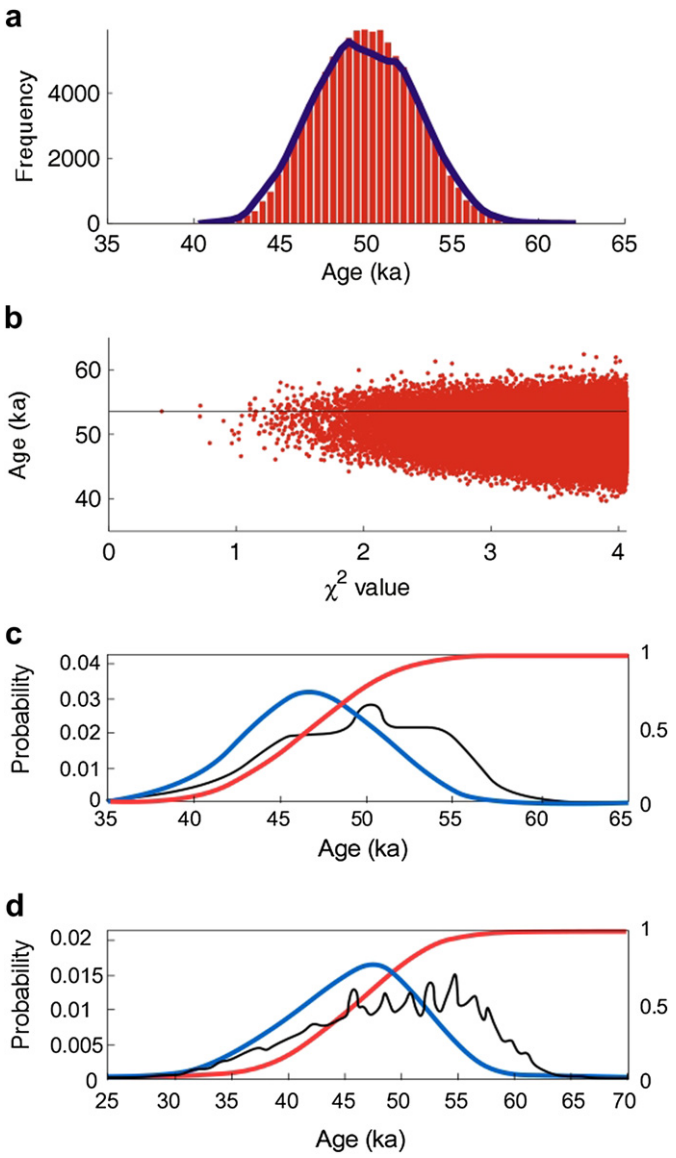

Fig. 12. Model 1 age results assuming simple single stage exposure. a. Frequency distribution of ages of the 100,000 curves for ^{26}Al measured in the Luchamange Beds (see Fig. 11A). Details of model parameters and constraints provided in SD4. b. Age versus χ^2 graph for the same ^{26}Al profile. Horizontal line indicates the age with the lowest χ^2 value. c. Smoothed χ^2 (thin black curve), probability density functions (blue), and cumulative distribution functions (red curve) for the depositional age of the Luchamange Beds based on the same ^{26}Al profile. d. Same as previous but for the ^{10}Be profile. (For interpretation of the references to color in this figure legend, the reader is referred to the web version of this article.)

sediment—as opposed to a more exotic eolian or littoral provenance—supports our interpretation that the capping sands are the result of local gully overbank sedimentation or the distal part of a small alluvial fan deposited on the bench.

4.2.2. Model 2. Multi-stage deposition and exposure

For a more robust calculation of the occupation age, Model 2 was constrained as follows:

(i) a 1.2 ± 0.3 m abrupt erosion event just prior to human presence. This was constrained trigonometrically according to these observations: i) the regional slope of the Luchamanage Beds is 5.5° west, ii) Mvumu's bench slopes <1° west, iii) this bench appears cut into the Luchamange Beds, and iv) sampling location at grid E1 (Figs. 4 and 6) on the easternmost side where the eroded thickness is greatest) (Fig. 13).
(ii) a short occupancy period (one century) based on the interpretation of the lithic assemblage as reflecting brief occupation at a quarry.
(iii) a 5 ± 3 ka age for the capping alluvial sand deposit, based on the ^{10}Be profile age and soil development.

Based on lowest chi-square fit of 100,000 curves (see SD3) the most probable age for the deposition of the Luchamange Beds (**Event 1**) is $42^{+77}/_{-15}$ ka (27–119 ka is 2σ range, Fig. 14A), however it is possible they were deposited over an extended period of time. As expected, this age is slightly younger than the apparent ages of 47.8 and 46.7 ka calculated on the ^{10}Be and ^{26}Al profiles, respectively, with Model 1, because in the Model 2 calculation, the fact that the Luchamange Beds were shallower for a short time prior to **Event 4** and therefore had a relatively higher production rate than today was considered.

The most probable age for the stochastically modelled abrupt erosion event (**Event 2**) is $29^{+3}/_{-11}$ ka (18–32 ka 2σ; Fig. 14C,D). The most probable timing of occupancy represented by the cultural layer is shortly after the age of the abrupt erosion event, because of the immediate juxtaposition of the cultural layer above the unconformity with no palaeosol or hiatus. We thus interpret the age modelled for **Event 2** as the age of MSA occupation.

5. Discussion

A cultural LSA affiliation for the lithics entrained in the upper Luchamange Beds, an iron pan underlying many of the archaeological assemblages on the Niassa-Malawi lakeshore, is not feasible because of the large size of detached products, high frequency of radial cores and points, blade absence, scarce microliths, and limited use of bipolar technology (Diez-Martín et al., 2009). The application of specific technological schemes to quartz reduction produces consistent morphotypes (Mehlman, 1989; Mercader et al., 2009) and the expedient character of regional MSA technologies is not a consequence of quartz brittleness alone. The rarity of bipolar

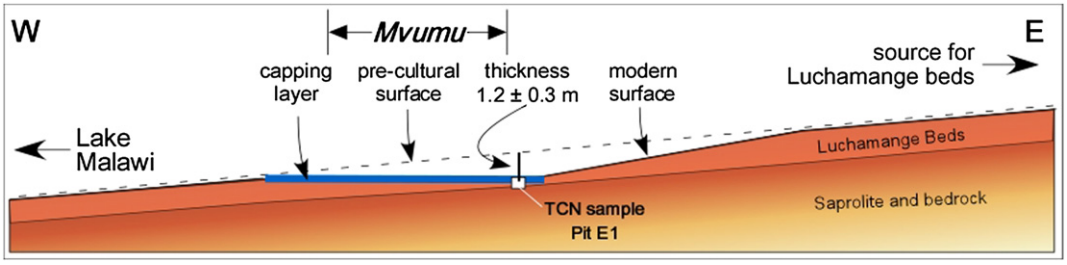

Fig. 13. West-east schematic cross section of Mvumu, indicating position of Pit E1 depth profile in the Luchamange Beds, and the trigonometric constraint on thickness of Luchamange Beds removed during the erosion event that formed the Mvumu bench.

technique is not related to variations in quartz quality. All known lithic assemblages from Niassa include examples of the finest conchoidal rocks, but these are irrelevant in the overall make-up despite their ready availability. Mvumu's raw materials other than quartz amount to <5% of the total, and all of them can be found within the surrounding Proterozoic crystalline basement or bordering Karoo outcrops located only 10–25 km away. Furthermore, "fine" materials exhibit identical techno-typological features to those seen in quartz. Massive pegmatite sheets cut through the crystalline basement and these exposures yield quartz blocks of the ideal size for quarrying and blank procurement. The low percent of stream-worn cortical surfaces confirms that pegmatitic quartz was favoured. Rounded cobbles from riverbeds, lake beaches, and residual Karoo conglomerates were exploited secondarily, but they came from the same general vicinity in the landscape where vein quartz was located.

Unfortunately, many MSA sites from tropical southern and east Africa do not have firm chronologies or lithic morphometrics that

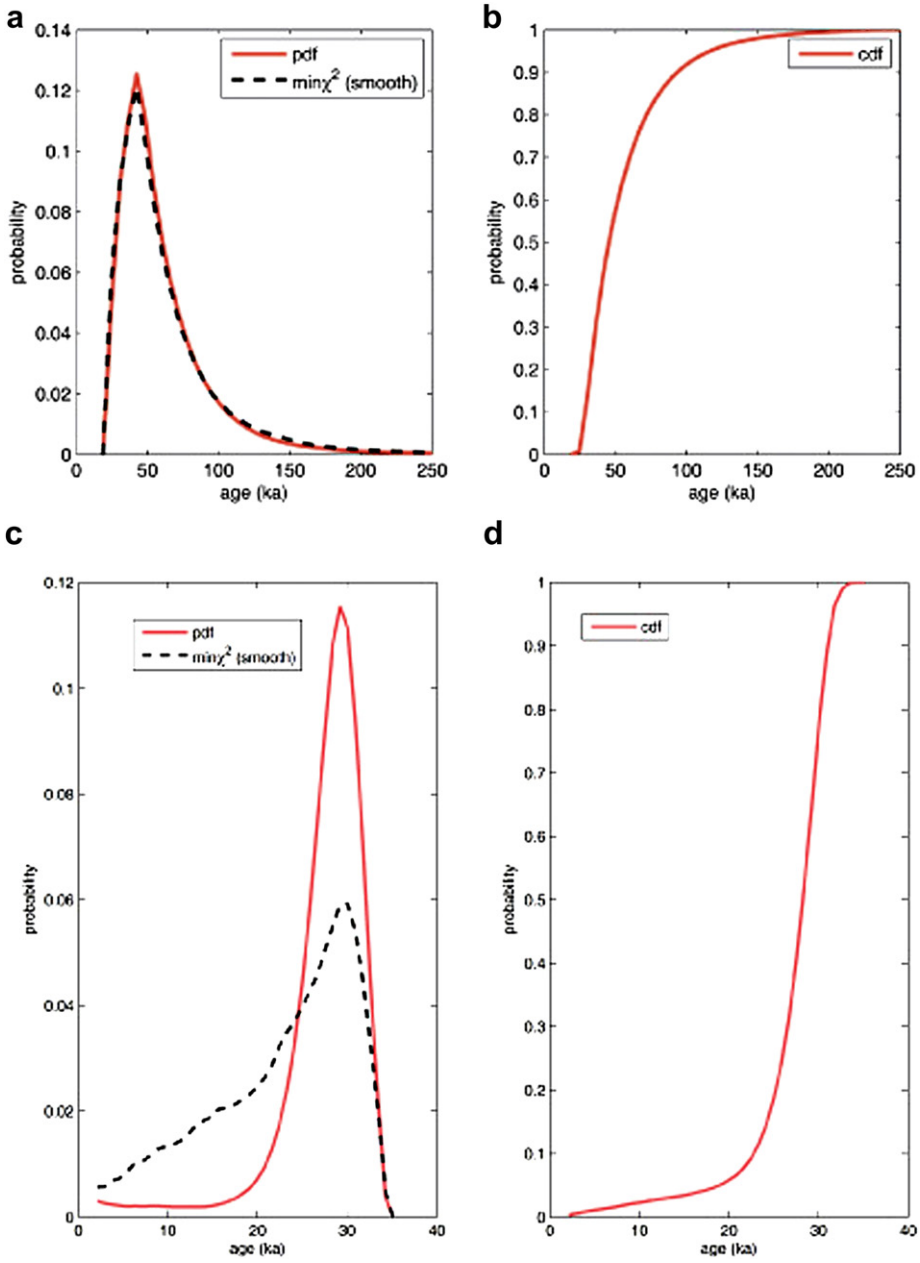

Fig. 14. Age results for Model 2 with multi-staged deposition and exposure history. Details of the model parameters and constraints provided in SD4 and SD5. A. Relative probability density function (pdf, blue curve) with minimum modelled chi-squared value (black dashed curve) and cumulative distribution function (cdf, red curve) for the depositional age of the Luchamange Beds. Solution obtained from 1 million iterations of the Monte Carlo-based model provided in SD4 and output provided in SD5. Probabilities are determined by obtaining a chi-squared statistic for each solution, weighting each solution by the chi-squared likelihood function, and averaging the probability at each age at a 0.1 ka interval. The most probable value of 42 ka is acquired from the maximum value on the pdf; asymmetric 2σ errors are obtained from cdf values at 0.046 and 0.954 for lower and upper errors and yield ages of 27 ka and 119 ka, respectively. B. Probability and minimum χ^2 curves (as above) for the age of the 90–150 cm erosion event that formed the bench upon which the cultural layer lies unconformably. The most probable value of 29 ka is acquired from the maximum value on the pdf; asymmetric 2σ errors are obtained from cdf values at 0.046 and 0.954 for lower and upper errors and yield ages of 18 ka and 32 ka, respectively. This represents the maximum age of occupancy at the Mvumu site. C. Frequency and probability distributions (graphs as per a,b) for the five 10Be measurements in the capping sand deposit. (For interpretation of the references to color in this figure legend, the reader is referred to the web version of this article.)

Table 6
Comparison of techno-typological components between the Niassa MSA lithics and those from Mumba (northern Tanzania).

Techno-typological feature	Niassa lakeshore (Mvumu and Mikuyu)[a,b,c]	Niassa highlands (Ngalue)[d]	Mumba, Bed VIb: Sanzako[e]	Mumba, Bed VIa: Kisele[e]
Raw materials, local	X	X	Insufficient data	Insufficient data
% Quartz, dominant	X	X	X	X
Simple cores, underexploited	X	–	–	–
Prepared cores	X	X	X	X
Blades, rare	X	X	X	X
Bipolar, rare	X	X	X	X
Bifacial reduction, rare	X	X	X	X
Tool, non-standardized; especially scrapers	X	X	X	X
Scrapers, common	X	X	X	X
Awls, present	X	X	X	X
Points, present	X	X	X	X
Microliths, rare	X	X	X	X
Large core tools; e.g. picks	X	X	X	X

[a] Mercader et al. (2008).
[b] Bennett (2011).
[c] This paper.
[d] Mercader et al. (2009).
[e] Mehlman (1989).

can be meaningfully assessed to establish cultural variation across space and industrial relationships governing ancient technological behaviour. This problem is especially pronounced with regards to Malawi; the natural extension of the study area. However, the new age estimates and interpretation of Mumba (Tanzania) constitute an exception and do represent a departure from traditional interpretations of the MSA-LSA transition (Gliganic et al., 2012) (Table 6). From a purely techno-typological perspective, the lithics from the Niassa highlands (Mercader et al., 2009) and lowlands (this paper) largely coincide with those described for the Kisele industries from Mumba's Bed VIa (Mehlman, 1989; Willoughby, 2009) at 63.4 ± 5.9 ka (Gliganic et al., 2012), but also with the underlying Sanzako industry from Bed VIb (Table 6) These are non-microlithic industries based on simple and prepared core technologies, mostly in quartz, with scrapers and points, and an infrequent use of bipolar technology. Importantly, all of the Mozambican industries across the region (Mercader et al., 2008, 2009, this paper: Figs. 7 and 8) and the Tanzanian Sanzako industry (Mehlman, 1989) do contain larger core tools resembling materials classically assigned to the Sangoan. That is, the regional expression of the Mozambican industries overlaps with the Tanzanian data from Mumba's Bed VIa and VIb from a fully technological perspective and, in the case of the Niassa highlands, from a temporal point of view as well. However, the age of the lowland Middle Stone Age industries from sites by the lake shore at 29 ka is at least 31 ka younger than the chronology recently established for the onset of the Later Stone Age at Mumba (Gliganic et al., 2012).

6. Conclusions

Absolute dating of Mvumu records MSA lakeshore occupation around 29 ka, during MIS 3. This age estimate is a benchmark for a prevalent relict geological formation in the Niassa-Malawi basin and is the first of its kind for any Mozambican MSA open air site. The organization of technology is expedient and non-standardized, with indiscriminate blank selection for tool manufacturing. Simple reduction dominates, microlithic techniques are rare, and there is no evidence of true blade production. Special purpose tools are limited to points and awls. Identical lithic repertoires from earlier MSA records from the cave sites in the adjacent temperate and humid highlands have been dated to 105–42 ka (Mercader et al., 2009). There is no evidence for a differential resource mobilization favouring conchoidal rock selection or the existence of long distance networks. The techno-typological profile from Mvumu is identical to that of other regional MSA sites known to span MIS 5, 4 and 3. This fact urges caution when building regional chronology from undated surface and excavation collections because they represent more than 70,000 years of technological persistence whereby ancestral morphotypes were still in use through the final phases of the MSA and persevered well into the chronological realm of the LSA.

Acknowledgements

We are grateful to Arianna Fogelman, Lourenço Thawe, Mussa Raja, Hilário Madiquida and the numerous workers, friends, and authorities in Niassa. The authors thank the Dept. of Anthropology and Archaeology at Eduardo Mondlane University. Work in Niassa was conducted under two permits to Julio Mercader from Eduardo Mondlane University and the Ministry of Education and Culture (03-2003 and 01-2007). Guang Yang processed all of the ^{26}Al and ^{10}Be targets at the Dalhousie Geochronology Centre. We thank the Canada Research Chairs program and the Canada Foundation for Innovation (CFI grant 201550 and CFI/AIF grant 2061-1005052-1). The Faculty of Social Sciences, Dept. of Archaeology, and various internal programs at the University of Calgary made available financial and logistical support to the authors. The Social Sciences and Humanities Research Council of Canada (File no. 410-2007-0697; CID: 148244) assisted this project, and NSERC grants MRS-342052 and DG-239961 provided maintenance support for the DGC cosmogenic nuclide lab.

Appendix A. Supplementary material

Supplementary material associated with this article can be found, in the online version, at doi:10.1016/j.quascirev.2012.05.018.

References

Afonso, R., Marques, J., Ferrara, M., 1998. A Evolução Geológica de Moçambique: Uma Síntese. Lisbon.
Anderson, R.S., Repka, J.L., Dick, G.S., 1996. Explicit treatment of inheritance in dating depositional surfaces using *in situ* ^{10}Be and ^{26}Al. Geology 24, 47–51.
Armstrong, A.L., 1931. Rhodesian archaeological expedition (1929): excavation in Bambata cave and researches on prehistoric sites in southern Rhodesia. Journal of the Royal Anthropological Institute of Britain and Ireland 61, 239–276.
Balco, G., Stone, J.O., Lifton, N.A., Dunai, T.J., 2008. A complete and easily accessible means of calculating surface exposure ages or erosion rates from ^{10}Be and ^{26}Al measurements. Quaternary Geochronology 3, 174–195.

Barham, L., Phillips, W.M., Maher, B.A., Karloukovski, V., Duller, G.A.T., Jain, M., Wintle, A.G., 2011. The dating and interpretation of a Mode 1 site in the Luangwa Valley, Zambia. Journal of Human Evolution 60, 549–570.

Barham, L.S., 2000. The Middle Stone Age of Zambia, South Central Africa. Western Academic & Specialist Press, Bristol.

Belmont, P., Pazzaglia, F., Gosse, J., 2007. Cosmogenic ^{10}Be as a tracer for hillslope and channel sediment dynamics in the Clearwater River, western Washington State. Earth and Planetary Science Letters 264, 123–135.

Bennett, T., 2011. Middle Stone Age Lithic Technology at Mvumu, Niassa, Mozambique, Master's thesis. Department of Archaeology. University of Calgary, Calgary, Canada.

Bettis, E.A., 2007. Weathering profiles. In: Elias, S.A. (Ed.), Encyclopedia of Quaternary Science. Elsevier, pp. 2119–2120.

Betzler, c., Ring, U., 1995. Sedimentology of the Malawi rift: facies and stratigraphy of the Chiwondo Beds, northern Malawi. Journal of Human Evolution 28, 23–35.

Bjerkgård, T., Boyd, R., Henderson, I., Grenne, T., Melezhik, V., Sandstad, J.S., Solli, A., Tveten, E., Key, R.M., Smith, R., Jamal, D., Catuane, F., Lima, J., Manhica, V., Manuel, S., Moniz, A., 2007. Metangula-Macaloge-Chiconono. Scale 1:250,000. Ministério dos Recursos Minerais, Maputo.

Bromage, T., Schrenk, F., Juwayeyi, Y., 1995. Paleobiogeography of the Malawi rift: age and vertebrate paleontology of the Chiwondo Beds, northern Malawi. Journal of Human Evolution 28, 37–57.

Brooks, A., Nevell, L., Yellen, J., Hartman, G., 2006. Projectile technologies of the African MSA. In: Hovers, E., Kuhn, S. (Eds.), Transitions before the Transition. Springer, New York, pp. 233–255.

Campbell, M.C., Tishkoff, S.A., 2010. The evolution of human genetic and phenotypic variation in Africa. Current Biology 20, R166–R173.

Campbell, M.C., Tishkoff, S.A., 2008. African genetic diversity: Implications for human demographic history, modern human origins, and complex disease mapping. Annual Review of Genomics and Human Genetics 9, 403–433.

Chapola, L., Kaphwiyo, C., 1992. The Malawi rift: geology, tectonics and seismicity. Tectonophysics 209, 159–164.

Charreau, J., Blard, P.-H., Puchol, N., Avouac, J.-P., Lallier-Verges, E., Boulres, D., Braucher, R., Gallaud, A., Finkel, R., Jolivet, M., Chen, Y., Roy, P., 2011. Paleoerosion rates in Central Asia since 9 Ma: a transient increase at the onset of Quaternary glaciations? Earth and Planetary Science Letters 304, 85–92.

Clark, J.D., 1995. Introduction to research on the Chiwondo Beds, Northern Malawi. Journal of Human Evolution 28, 3–5.

Clark, J.D., 1966. Initial investigation of the Archeology of Karonga District, Malawi. American Anthropologist 68, 67–89.

Clark, J.D., Brown, K., 2001. The Twin Rivers Kopje, Zambia: stratigraphy, fauna, and artefact assemblages from the 1954 and 1956 excavations. Journal of Archaeological Science 28, 305–330.

Clark, J.D., Haynes, C.V., 1970. An elephant butchery site at Mwanganda's village, Korongo, Malawi, and its relevance for paleolithic archaeology. World Archaeology 1, 390–411.

Clark, J.D., Kleindienst, M., 2001. The stone age cultural sequence: terminology, typology, and raw materials. In: Clark, J.D. (Ed.), Kalambo Falls Prehistoric Site, vol. III. Cambridge University Press, Cambridge, pp. 34–65.

Cohen, A., Stone, J., Beuning, K., Park, L., Reinthal, P., Dettman, D., Scholz, C., Johnson, T., King, J., Talbot, M., Brown, E., Ivory, S., 2007. Ecological consequences of early late Pleistocene megadroughts in tropical Africa. Proceedings of the National Academy of Sciences of the United States of America 104, 16422–16427.

Crossley, R., 1986. Sedimentation by termites in the Malawi rift valley. Geological Society Special Publication 25, 191–199.

da Barka, A., dos Santos, T., 2005. Geografia de Moçambique. Diname, Maputo.

Diez-Martín, F., Domínguez-Rodrigo, M., Sánchez, P., Mabulla, A., Tarriño, A., Barba, R., Prendergast, M., de Luque, L., 2009. The Middle to Later Stone Age technological transition in East Africa. New data from Mumba Rockshelter bed V (Tanzania) and their implications for the origin of modern human behavior. Journal of African Archaeology 7, 1–27.

Dixey, F., 1927. The Tertiary and post-Tertiary lacustrine sediments of the Nyassan Rift-valley. Quarterly Journal of the Geological Society of London 83, 432–437.

Ebinger, C.J., Reynolds, D.J., Rosendahl, B.R., 1987. Tectonic model for the Malawi rift, Africa. Tectonophysics 141, 215–235.

Flannery, J.W., Rosendahl, B.R., 1990. The seismic stratigraphy of Lake Malawi, Africa: implications for the interpreting of geological processes in lacustrine rifts. Journal of African Earth Sciences 10, 519–548.

Gliganic, L.A., Jacobs, Z., Roberts, R.G., Domínguez-Rodrigo, M., Mabulla, A.Z.P., 2012. New ages for Middle and Later Stone Age deposits at Mumba rockshelter, Tanzania: optically stimulated luminescence dating of quartz and feldspar grains. Journal of Human Evolution 62, 533–547.

Gibbon, R., Granger, D., Kuman, K., Partridge, T., 2009. Early Acheulean technology in the Rieputs formation, South Africa, dated with cosmogenic nuclides. Journal of Human Evolution 56, 152–160.

Heisinger, B., Lal, D., Jull, A.J.T., Kubik, P., Ivy-Ochs, S., Neumaier, S., Knie, K., Lazarev, V., Nolte, E., 2002a. Production of selected cosmogenic radionuclides by muons: 1. Fast muons. Earth and Planetary Science Letters 200, 345–355.

Heisinger, B., Lal, D., Jull, A.J.T., Kubik, P., Ivy-Ochs, S., Knie, K., Nolte, E., 2002b. Production of selected cosmogenic radionuclides by muons: 2. Capture of negative muons. Earth and Planetary Science Letters 200, 357–369.

Hidy, A.J., Gosse, J.C., Pederson, J.L., Mattern, J.P., Finkel, R.C., 2010. A geologically constrained Monte Carlo approach to modeling exposure ages from profiles of cosmogenic nuclides: an example from Lees Ferry, Arizona. Geochemistry Geophysics Geosystems 11. http://dx.doi.org/10.1029/2010GC003084.

Inizan, M.L., Reduron-Ballinger, M., Roche, H., Tixier, J., 1999. Technology and Terminology of Knapped Stone. CREP, Nanterre.

Isaac, G., 1977. Olorgesailie. Archaeological Studies of a Middle Pleistocene Lake Basin in Kenya. Univ of Chicago Press, Chicago.

Kaufulu, Z., 1990. Sedimentary environments at the Mwanganda site, Malawi. Geoarchaeology 5, 15–27.

Kaufulu, Z., Stern, N., 1987. The first stone artefacts to be found in situ within the Plio-Pleistocene Chiwondo beds in northern Malawi. Journal of Human Evolution 16, 729–740.

Lächelt, S., 2004. Geology and Mineral Resources of Mozambique. Direcção Nacional de Geologia, Maputo.

Lal, D., 1991. Cosmic ray labeling of erosion surfaces: *In situ* nuclide production rates and erosion models. Earth and Planetary Science Letters 104, 424–439.

Lifton, N., Bieber, J., Clem, J., Duldig, M., Evenson, P., Humble, J., Pyle, R., 2005. Addressing solar modulation and long term uncertainties in scaling secondary cosmic rays for *in situ* cosmogenic nuclide applications. Earth and Planetary Science Letters 239, 140–161.

Mehlman, M., 1989. Later Quaternary archaeological sequences in northern Tanzania. Ph. D. dissertation. University of Illinois, USA.

Mercader, J., Bennett, T., Raja, M., 2008. Middle Stone Age Starch Acquisition in the Niassa rift, Mozambique. Quaternary Research 70, 283–300.

Mercader, J., Asmerom, Y., Bennett, T., Raja, M., Skinner, A., 2009. Initial excavation and dating of Ngalue Cave: a Middle Stone Age site along the Niassa rift, Mozambique. Journal of Human Evolution 57, 63–74.

Moore, M.W., Sutikna, T., Jatmiko, Morwood, M., Brumm, A., 2009. Continuities in stone flaking technology at Liang Bua, Flores, Indonesia. Journal of Human Evolution 57, 503–526.

Nishiizumi, K., 2004. Preparation of ^{26}Al AMS standards. Nuclear Instruments and Methods in Physics Research B 223–224, 388–392.

Nishiizumi, K., Imamura, M., Caffee, M., Southon, J., Finkel, R., McAnich, J., 2007. Absolute calibration of ^{10}Be AMS standards. Nuclear Instruments and Methods in Physics Research B 258, 403–413.

Perg, L.A., Anderson, R.S., Finkel, R.C., 2001. Use of a new ^{10}Be and ^{26}Al inventory method to date marine terraces, Santa Cruz, California, USA. Geology 29, 879–882.

Pinna, P., Marteau, P., Manigault, B., Becogirodon, G., 1987. Carta Geólogica da República Popular de Moçambique, 1:1000000. ING, Maputo.

Plug, L.J., Gosse, J.C., McIntosh, J.J., Bigley, R., 2007. Attenuation of cosmic ray flux in temperate forest. Journal of Geophysical Research 112, F02022.

Reid, I., Frostick, E., 1986. Slope processes, sediment derivation and landform evolution in a rift valley basin, Northern Kenya. Geological Society Special Publication 25, 99–111.

Ring, U., Betzler, C., 1995. Geology of the Malawi rift: kinematic and tectonosedimentary background to the Chiwondo Beds, northern Malawi. Journal of Human Evolution 28, 7–21.

Rood, D.H., Hall, S., Guilderson, T., Finkel, R., Brown, T., 2010. Challenges and opportunities in high-precision Be-10 measurements at CAMS. Nuclear Instruments and Methods in Physics Research B: Beam Interactions with Materials and Atoms.

Salman, G., Abdula, E., 1995. Development of the Mozambique and Rovuma sedimentary basins, offshore Mozambique. Sedimentary Geology 96, 7–41.

Sandrock, O., Kullmer, O., Schrenk, F., Juwayeyi, Y., Bromage, T., 2007. Fauna, taphonomy, and ecology of the Plio-Pleistocene Chiwondo Beds, Northern Malawi. In: Bobe, R., Alemseged, Z., Behrensmeyer, A. (Eds.), Hominin Environments in the East African Pliocene: An Assessment of the Faunal Evidence. Springer, New York, pp. 315–332.

Specht, T., Rosendahl, B., 1987. Architecture of the Lake Malawi Rift, East Africa. Journal of African Earth Sciences 8, 355–382.

Staiger, J., Gosse, J., Toracinta, R., Fastook, J., Johnson, J., 2007. Atmospheric scaling of cosmogenic nuclide production: climate effect. Journal of Geophysical Research 112 (B2). http://dx.doi.org/10.1029/2005JB003811.

Stephens, E., 1966. Geological account of the northwest coast of lake Malawi between Karonga and Lion Point, Malawi. American Anthropologist 68, 50–58.

Stone, J.O., 2000. Air pressure and cosmogenic isotope production. Journal of Geophysical Research 105, 753–759.

Thompson, J., Mackay, A., Wright, D.K., Welling, M., Greaves, A., Gomani-Chindebvu, E., Simengwa, D., Renewed investigations into the Middle Stone Age of northern Malawi. Quaternary International. in press.

Timberlake, J.R., Golding, J.S., Smith, P., 2006. A preliminary analysis of endemic and threatened plants of the Flora Zambesiaca area. In: Ghazanfar, S.A., Beenje, H. (Eds.), Taxonomy and Ecology of African Plants and Their Conservation and Sustainable Use. Royal Botanical Gardens, Kew, pp. 749–760.

Verniers, J., Paulis, R., Frasca, S., Jourdan, P., 1978. Relatório da brigada geológica de cartografía da bacia carbonífera de Maniamba. DINAGECA, Maputo.

White, F., 1983. The Vegetation of Africa: a Descriptive Memoir to Accompany the Unesco/Aetfat/Unso Vegetation Map of Africa, Natural Resources Research. Unesco, Paris, p. 336.

Willoughby, P., 2009. From Middle to Later Stone Age in Eastern Africa. In: Camps, M., Chauhan, P. (Eds.), Sourcebook of Paleolithic Transitions. Springer, New York, pp. 301–314.